Tellus (2001), 53B, 479–490
Printed in UK. All rights reserved

Copyright © Munksgaard, 2001
TELLUS
ISSN 0280–6509

On the formation, growth and composition of nucleation mode particles

By M. KULMALA*, M. DAL MASO, J. M. MÄKELÄ, L. PIRJOLA, M. VÄKEVÄ, P. AALTO, P. MIIKKULAINEN, K. HÄMERI and C. D. O'DOWD, *University of Helsinki, Department of Physics, PO Box 64, Fin-00014 Helsinki, Finland*

(Manuscript received 2 May 2000; in final form 8 March 2001)

ABSTRACT

Taking advantage of only the measured aerosol particles spectral evolution as a function of time, a new analytical tool is developed to derive formation and growth properties of nucleation mode aerosols. This method, when used with hygroscopic growth-factors, can also estimate basic composition properties of these recently-formed particles. From size spectra the diameter growth-rate can be obtained, and aerosol condensation and coagulation sinks can be calculated. Using this growth-rate and condensation sink, the concentration of condensable vapours and their source rate can be estimated. Then, combining the coagulation sink together with measured number concentrations and apparent source rates of 3 nm particles, 1 nm particle nucleation rates and concentration can be estimated. To estimate nucleation rates and vapour concentration source rates producing new particle bursts over the Boreal forest regions, three cases from the BIOFOR project were examined using this analytical tool. In this environment, the nucleation mode growth-rate was observed to be 2–3 nm $hour^{-1}$, which required a condensable vapour concentration of $2.5–4 \times 10^7$ cm^{-3} and a source rate of approximately $7.5–11 \times 10^4$ $cm^{-3}\,s^{-1}$ to be sustained. The formation rate of 3 nm particles was ≈ 1 particle $cm^{-3}\,s^{-1}$ in all three cases. The estimated formation rate of 1 nm particles was 10–100 particles $cm^{-3}\,s^{-1}$, while their concentration was estimated to be between 10,000 and 100,000 particles cm^{-3}. Using hygroscopicity data and mass flux expressions, the mass flux of insoluble vapour is estimated to be of the same order of magnitude as that of soluble vapour, with a soluble to insoluble vapour flux ratio ranging from 0.7 to 1.4 during these nucleation events.

1. Introduction

Aerosol particles are ubiquitous in the Earth's atmosphere and affect our quality of life through many different processes. In polluted urban environments, aerosol emissions can affect public health through their inhalation (Donaldson et al., 1998), whilst further away from urban sources, aerosols are thought to contribute to climate change patterns (Charlson et al., 1987). In recent years, considerable effort has been devoted to understanding how aerosols directly affect the earth's radiation budget through direct back scatter of incoming solar radiation, thus contributing to a planetary cooling. Not only do aerosols directly affect the radiation budget, they also contribute to this budget indirectly through the formation of clouds. It is generally considered that an increase of aerosols will lead to brighter and more sustained cloud cover, thus providing additional planetary cooling.

The formation and growth of atmospheric aerosols are key processes determining the dynamics of atmospheric aerosols. In order to be able to better understand the health and climatic effects

* Corresponding author.
e-mail: markku.kulmala@helsinki.fi

of atmospheric aerosols, their formation processes should also be better understood. Nucleation, the formation of ultrafine particles detected at a few nm, and subsequent growth to $\sim$100 nm in 1–2 days, has been observed frequently in the continental boundary layer. Such observations span from northern-most sub-arctic Lapland, over the remote boreal forest (Mäkelä et al., 1997; Kulmala et al., 1998) and suburban Helsinki (Väkevä et al, 2000), to industrialised agricultural regions in Germany (Birmili and Wiedensohler, 1998) and also to coastal environments around Europe (O'Dowd et al., 1999). The atmospheric new particle formation rates have also been investigated by Weber et al. (1996, 1997), and the biogenic aerosol formation by Kavouras et al. (1998). For quantification and predictive purposes, it is important to understand the underlying processes leading to the formation and evolution of atmospheric aerosols.

In this study, to obtain some physical and chemical insight into natural aerosol formation processes, a simple analytical method is developed to estimate (a) the concentration of condensable vapour leading to observed particle growth; (b) it's source strength; (c) the formation rate of 3 nm particles, which is the minimum detectable size of aerosol particles using state-of-art aerosol instrumentation; and (d) the formation rate and number concentration of 1 nm, i.e., the presumed size of newly formed particles. This analysis is performed using only size distribution data during nucleation and growth events with particular attention to condensation and coagulation sinks. Additionally, the ratio between concentrations of soluble and insoluble condensable vapour fluxes can be obtained by integrating measured hygroscopic growth-factors into the analytical approach. This method is used to evaluate new particle and growth events observed in the boreal forest regions where the BIOFOR (Biogenic Aerosol Formation over the Boreal Forest) project was conducted from 1998–2000 (Kulmala et al., 2001). Three BIOFOR intensive field campaigns took place in Hyytiälä (61°51′N 24°17′E) in the Boreal forest region of central southern Finland. Hyytiälä is also the site for the Finnish SMEAR II station (Station for Measuring forest Ecosystem-Atmospheric Relations) hosting continuous long-term monitoring of atmospheric processes such as turbulent fluxes and aerosol physico-chemical interactions, which allow the general BIOFOR results to be viewed in the context of annual cycles and inter annual variability.

2. Analytical tools to estimate aerosol and vapour properties from experimental data

2.1. Basic equations

The observed nucleation mode growth, the source rate of condensable material and the changes of hygroscopic properties during the nucleation and growth events are analysed using three equations describing the rate of change of vapour concentration, aerosol particle number concentration and particle growth. Considering condensable vapour molecules of species X, the time dependence of the vapour concentration (C) can be expressed (see also Kulmala et al., 1998) by

$$\frac{\mathrm{d}C}{\mathrm{d}t} = Q - \mathrm{CS} \cdot C, \tag{1}$$

where Q is the source rate of the vapour and CS is its condensation sink (in more detail see Subsection 2.2) to the pre-existing aerosol. The time evolution for aerosol number concentration (N) in size class i can be presented by:

$$\frac{\mathrm{d}N_i}{\mathrm{d}t} = J_i - \mathrm{CoagS} \cdot N_i, \tag{2}$$

where J_i is the formation rate of particles and CoagS is the coagulation sink (see Subsection 2.3) both for size i particles. The growth-rate can be expressed (Kulmala, 1988):

$$\frac{\mathrm{d}r}{\mathrm{d}t} = \frac{m_\mathrm{v}\beta_\mathrm{m}\mathrm{DC}}{r\rho}. \tag{3}$$

Here, r is particle radius, m_v is molecular mass of condensable vapour, β_m is transitional correction factor for mass flux (given in Subsection 2.2), D is diffusion coefficient, and ρ is particle density. The eq. (3) can be integrated from r_0 to r to obtain:

$$C = \rho \left\{ \frac{r^2 - r_0^2}{2} + [4/(3\alpha) - 0.623]\lambda(r - r_0) + 0.623\lambda^2 \ln \frac{\lambda + r}{\lambda + r_0} \right\} \Big/ \Delta t D m_\mathrm{v}. \tag{4}$$

Here, α is mass accommodation coefficient (i.e., sticking probability) and λ is the mean free path.

Directly from measurements of the aerosol size distribution changes and hygroscopicity properties, dr/dt, CS, CoagS, $dN_{3\,nm}/dt$, $N_{nucleation\ mode}$, and the soluble fraction can be obtained.

Using the above mentioned equations and the experimental data, we are also able to determine J_1 (nucleation rate, or formation rate, for 1-nm particles) where 1 nm is assumed to be the size of a new particle. N_1 is the number concentration of 1 nm particles N_3 is number concentration of 3 nm particles. J_3 is formation rate of 3 nm particles. In order to obtain J_1, we develop a 5-step derivation of J_1.

First, an expression for N_1 is required:

$$\frac{dN_1}{dt} = J_1 - K_1 N_1 - J_3, \tag{5}$$

where K_1 is the coagulation sink for 1 nm particles. In practise, it is the coagulation between 1 nm particles and larger particles of size distribution. Then, assuming a steady-state situation,

$$J_1 = K_1 N_1 + J_3. \tag{6}$$

Second, the link between $K_1 N_1$ and J_3 can be determined using the fact that a fraction of N_1 particles will coagulate before they enter the 3 nm size range.

Coagulation of N_1 during the growth from 1 nm to 3 nm can be obtained from

$$\frac{dN_{1,3}}{dt} = -KN_{1,3} \Rightarrow \frac{dN_{1,3}}{N_{1,3}} = -K\,dt \Rightarrow N_{1,3} = N_1 e^{-Kt}. \tag{7}$$

Here, $N_{1,3}$ corresponds the concentration of particles growing from 1 to 3 nm, t is the growth time and K is their coagulation sink. So the fraction of N_1 coagulated during the growth is $1 - e^{-Kt}$, and the fraction of N_1 contributing to J_3 is e^{-Kt}. Therefore

$$\frac{K_1 N_1}{J_3} \cong \frac{1 - e^{-Kt}}{e^{-Kt}} = e^{Kt} - 1 \tag{8}$$

and $\quad K_1 N_1 = J_3(e^{Kt} - 1).$

Third, combining the above for J_1:

$$J_1 = K_1 N_1 + J_3 = J_3(e^{Kt} - 1) + J_3 = J_3 e^{Kt}. \tag{9}$$

Fourth, since the equation for N_3 is

$$\frac{dN_3}{dt} = J_3 - K_3 N_3, \tag{10}$$

then

$$\Rightarrow J_3 = \frac{dN_3}{dt} + K_3 N_3. \tag{11}$$

Finally, J_1 is given by

$$J_1 = J_3 e^{Kt} = \left[\frac{dN_3}{dt} + K_3 N_3\right] e^{Kt}. \tag{12}$$

The time t in equations above corresponds to the particle growth time for 1 nm to grow to 3 nm and K is a typical coagulation sink during the growth, the actual value of which is close to K_1.

In practice, dN_3/dt and N_3 are the observed formation rate of 3 nm particles and the number concentration of nucleation mode particles (larger than 3 nm). Therefore also in equation (10) there is no condensational transport term that would move particles to larger sizes.

2.2. *Condensation sink*

The aerosol condensation sink determines how rapidly molecules will condense onto pre-existing aerosols and depends strongly on the shape of the size distribution (Pirjola et al., 1999). As an example, the concentration of sulphuric acid [SA], which is determined by chemical production, nucleation and condensation, can be expressed by

$$\frac{d[SA]}{dt} = k \cdot [OH] \cdot [SO_2] - J \cdot n^* - 4\pi CS \cdot D \cdot ([SA] - [SA]_r), \tag{13}$$

where k is the chemical reaction rate constant, J is the nucleation rate and n^* is the number of sulphuric acid molecules in the critical cluster. The condensation sink (CS) is $4\pi D\,CS'$, and CS' is integrated over the aerosol size distribution:

$$CS' = \int_0^\infty r\beta_M(r)n(r)\,dr = \sum_i \beta_{M_i} r_i N_i. \tag{14}$$

Here, the transitional correction factor can be expressed (Fuchs and Sutugin, 1971)

$$\beta_M = \frac{Kn + 1}{0.377Kn + 1 + \frac{4}{3}\alpha^{-1}Kn^2 + \frac{4}{3}\alpha^{-1}Kn}. \tag{15}$$

The Knudsen number is

$$Kn = \frac{\lambda_v}{r},$$

and the sticking coefficient α is typically assumed

to be unity. In the molecular regime where $Kn \gg 1$ we have

$$\beta_{\mathrm{M}} \approx \frac{3r}{4\lambda_{\mathrm{v}}} \qquad \text{and} \qquad \mathrm{CS} \propto r^2.$$

On the other hand, in the continuum regime where $\mathrm{Kn} \ll 1$, we get

$$\beta_{\mathrm{M}} = 1 \qquad \text{and} \qquad \mathrm{CS} \propto r.$$

However, typical tropospheric aerosol also occupy the transitional regime and $\mathrm{CS} \propto r^a$ where $1 < a < 2$.

2.3. *Coagulation sink CoagS*

The coagulation sink determines how rapidly nm-size aerosol particles are removed through coagulation. The coagulation sink can be determined from

$$\mathrm{CoagS} = \sum_j K_{ij} N_j. \tag{16}$$

Here K_{ij} is the coagulation coefficient (Fuchs, 1964; Seinfeld and Pandis, 1998) which in the transitional regime is:

$$K_{12} = \frac{K_{\mathrm{C}}^{\mathrm{B}}}{\dfrac{R_{12}}{R_{12}+\sigma_{12}} + \dfrac{4D_{12}}{\bar{c}_{12}R_{12}}}, \tag{17}$$

where $K_{\mathrm{C}}^{\mathrm{B}} = 4\pi(R_1 + R_2)(D_1 + D_2)$ is the coagulation coefficient in the continuum regime,

$$D_i = \frac{kTC_{\mathrm{C}}}{6\pi\mu R_i}$$

is the particle diffusion coefficient, and μ is the gas dynamic viscosity.

The Cunningham correction factor is given by $C_{\mathrm{C}} = 1 + \mathrm{Kn}(\alpha_1 + \alpha_2 \exp(-\alpha_3/\mathrm{Kn}))$, where Kn is calculated for air and $\alpha_1 = 1.142$, $\alpha_2 = 0.558$ and $\alpha_3 = 0.999$ (Allen and Raabe, 1985).

In the coagulation coefficient, $R_{12} = R_1 + R_2$, $D_{12} = D_1 + D_2$, and

$$\bar{c}_{12} = \sqrt{\bar{c}_1^2 + \bar{c}_2^2}$$

is mean relative thermal velocity between the particles,

$$\bar{c}_i = \sqrt{\frac{8kT}{\pi m_i}}$$

is average velocity of particle i with mass m_i,

$$\sigma_{12} = \sqrt{\omega_1^2 + \omega_2^2}$$

is the distance at which the two fluxes are matched,

$$\omega_i = \frac{(R_{12} + \gamma_i)^3 - (R_{12}^2 + \gamma_i^2)^{3/2}}{3R_{12}\gamma_i} - R_{12},$$

$$\gamma_i = \frac{8D_i}{\pi\bar{c}_i}$$

(Fuchs, 1964).

3. Aerosol size-distribution and hygroscopicity measurements

During the BIOFOR intensive field campaigns, total particle concentration was determined using a pair of TSI Condensation Particle Counters (CPCs) measuring concentrations at sizes larger than 3 nm (TSI 3025) and 10 nm (TSI 3010). Submicron size distributions were taken using a dual DMPS (Differential Mobility Particle Sizer) system covering sizes of 3–10 nm and 10–500 nm, respectively. The ultra-fine DMPS comprised an 11 cm long Vienna-type DMA (Differential Mobility Analyzer) (Winklmayr et al., 1991) and a TSI 3025 CPC (Stolzenburg and McMurry, 1991). The DMPS covering Aitken mode and accumulation mode sizes comprised a 28 cm long DMA and a TSI 3010 CPC (Quant et al., 1992) and measured particles between 10 and 500 nm diameter. The primary aerosol intake flow was approximately 25 $\mathrm{m^3\,h^{-1}}$, from which a sample flow of 5 LPM was taken to the DMPS. The aerosol was brought into charge equilibrium with a bipolar Kr85 aerosol neutraliser (TSI model 3077)

For the data analysis, charging probabilities by Wiedensohler (1988) and DMA transfer functions by Stolzenburg (1988) were used. The CPC detection efficiencies and DMA diffusion losses were determined experimentally with silver particles (Aalto et al., 2001). The sampling line losses were calculated using laminar flow diffusion theory. The calculated DMPS kernel matrix was inverted using pseudo-inversion method. DMPS particles were sampled as dry, dehydraded, particles and were later converted to "ambient" hydrated sizes using experimentally determined particle growth-factors.

Accumulation mode and coarse mode ambient size distributions were taken using in-situ optical particle counters. Sizes from 100 nm to 3 μm were taken using a Particle Measuring System's (PMS)

Active Scattering Aerosol Spectrometer Probe (ASASP-300), while super-micron distributions were taken using a PMS Classical Scattering Aerosol Spectrometer Probe (CASAP-100), covering sizes from 0.5 μm to 32 μm diameter.

Particle growth-factor responses to relative humidity were investigated to elucidate the physico-chemical and soluble characteristics of recently-formed and developing new particle modes. A Tandem Differential Mobility Analyzer (TDMA) was used to study the particle size response to humidity (Hämeri et al., 2000). The instrument provides a novel way for in-situ determination of chemical characteristics of individual aerosol particles. A TDMA has a good time resolution (10 minutes) and can be used even with rather low concentrations. During the BIOFOR campaigns an Ultrafine-TDMA system (UF-TDMA) was used to study hygroscopic growth-factors of particles smaller than 30 nm in mobility diameter (Hämeri et al., 2001). Measurements of the hygroscopic properties provided also size-resolved, in-situ information on the state of mixing (external/internal mixing).

The basic operational principle is to select a narrow size fraction from dry ambient aerosol, humidify the selected particles in a controlled environment, and study the change in particle mobility diameter due to water uptake. The result is described with a diameter growth-factor, i.e., the ratio between particle diameter at 90% relative humidity and dry conditions. From the diameter growth-factor the amount of soluble material, i.e., the soluble volume fraction (ε), can further be estimated. This is done using the following equation

$$\varepsilon = \frac{(\mathrm{GF}^3 - 1)}{(\mathrm{GF}_\mathrm{A}^3 - 1)}, \tag{18}$$

where GF is the diameter growth-factor at 90% relative humidity, and $\mathrm{GF_A}$ is the growth-factor of a reference salt particle with the same size. As the reference calibration salt, $(NH_4)_2SO_4$ was used. The validity of the use of ammonium sulphate as the reference salt was investigated by Hämeri et al. (2001) who found good agreement with calculations of growth based on the use of ionic composition from impactor samples. A more detailed discussion and evaluation on the aerosol instrumentation used during BIOFOR is given in Aalto et al. (2001).

4. Results and discussion

4.1. Data analysis

3 nucleation event days during the third BIOFOR campaign in April 1999 were selected for analysis. Sub-micron size distribution data for these days all show a clear increase of small particle (<10 nm) concentration during the late morning, and their subsequent growth into Aitken mode and accumulation mode sizes throughout the afternoon and into the evening. For each event period, the start and end times of the event, and the maximum size reached by the newly-formed particles after the end of the growth event were determined from the experimental data. Using these observations, estimates of the number of newly formed particles were made. $\mathrm{d}N_3/\mathrm{d}t$, the apparent nucleation rate or appearance rate of 3 nm particles, was determined by taking the observed concentration of newly formed particles and dividing it by the formation time. Typical values of the apparent nucleation rate throughout the whole campaign range from 0.1 to 1 $\mathrm{cm^{-3}\,s^{-1}}$ and are discussed further in Mäkelä et al. (2000) where a more in-depth analysis of these events is presented.

An example of the typical ultra-fine size distribution growth, determined by the DMPS, is shown in Fig. 1 for JD 104 (14 April 1999). Around noon, there is a large increase in total number concentration from $\approx 2000\ \mathrm{cm^{-3}}$ to $\approx 10000\ \mathrm{cm^{-3}}$, typically following the breakup of a nocturnal boundary layer, leading to subsequent vigorous mixing with the residual boundary layer (Nilsson et al., 2001). Generally, the appearance of the new particle mode occurs after mixing, and the mixing time and the appearance time seem to agree with each other if the growth time from 1 nm to 3 nm is taken into account (Nilsson et al., 2001). This well-mixed meteorological condition suggests that the aforementioned steady-state assumptions hold, particularly since, after mixing, there are no sudden or significant injections of new particles or vapours due to mixing effects. The size spectra evolution illustrates the growth of the nucleation mode up to sizes of the order of 50–100 nm over periods of the order of 10 h, while total concentration reduces rapidly due to coagulation losses. As the particles grow out of the nucleation mode size

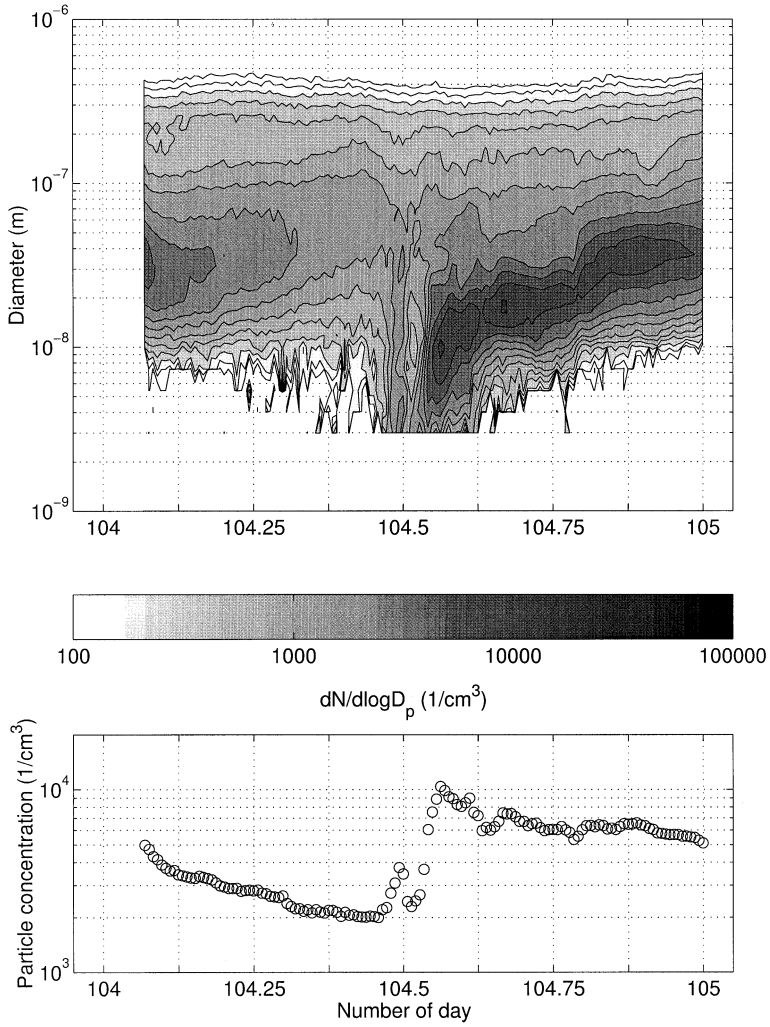

Fig. 1. Diurnal variation of aerosol size distribution, Hyytiälä 14 April 1999.

range, concentration loss reduces as coagulation becomes less effective for the larger sizes.

From these observations, the growth-rate, sinks and aerosol number concentration are determined. From the TDMA observations, the hygroscopic growth-factors and soluble fraction of the new particles are determined. The growth-rate was determined using the mean size of the nucleation mode particles at the beginning of particle formation event and two hours later. The coagulation sinks and condensation sink are determined from the combined distributions taken by the DMPS and optical particle counter size measurements. The coagulation coefficients for 1 nm, 2 nm and 3 nm particles with all larger size class were also calculated from the size distribution observations. The expression for J_1 depends exponentially on both the growth time of a particle to the 3 nm size and the coagulation sink used. The growth time from 1 nm to 3 nm was thus estimated from the growth-rate of the nucleation mode particles. For BIOFOR, the growth-rates were calculated to be from 2 to 4 nm/h in the three cases considered, and were used to calculate upper and lower estimates for J_1 and N_1. The higher the growth-rate the smaller the coagulation losses are during

the growth from 1 nm to 3 nm. The coagulation sink K, representing the removal of particles smaller than 3 nm, was taken as the average of the coagulation sink for 1 and 2 nm particles since most of the coagulation occurs in this size range.

4.2. Condensation and coagulation sinks

In Fig. 2, the condensation sink (with mass accommodation coefficient of the condensable vapour being unity), together with the coagulation sinks for Julian Day 104 (14 April) are displayed. Both the condensation and coagulation sinks behave in a similar fashion, with, at the start of the nucleation and growth event, a condensation sink of the order of $2.5 \times 10^{-2}\,\mathrm{cm}^{-3}\,\mathrm{s}^{-1}$, and a coagulation sink of the order of $1.5 \times 10^{-2}\,\mathrm{cm}^{-3}\,\mathrm{s}^{-1}$ for 1 nm particles, reducing to $2 \times 10^{-3}\,\mathrm{cm}^{-3}\,\mathrm{s}^{-1}$ for 3 nm particles.

The sub-micron DMPS data correspond to "dried" dehydrated aerosol sizes, while the super-micron distributions were taken at ambient humidity, and thus, ambient "wet" aerosol sizes. Consequently, the response of the ambient aerosol to humidity-induced growth will also be reflected in the calculated condensation sink. The effect of particle growth-factors on the calculated condensation sink is illustrated in Fig. 3a where the condensation sink as a function of size is calculated using growth-factors from 1 to 1.5 and an accommodation coefficient of 1. The peak condensation sink occurs for the accumulation mode for both growth-factors, suggesting that this mode contributes to the largest removal rate of ambient vapours. Increasing the growth- factor from 1 to 1.5 increases the condensation sink by a factor of 2, but does not significantly alter the location of the peak sink size. The actual growth-factor at ambient humidities were typically between 1 and 1.5. It should be noted that there is no change in the calculated sink for super-micron particles since these sizes are actual measured wet sizes.

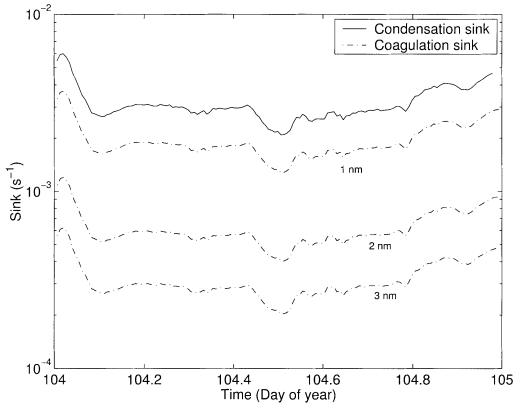

Fig. 2. Diurnal variation of condensation and coagulation (1 nm, 2 nm and 3 nm) sinks, Hyytiälä 14 April 1999.

The effect of choice of mass accommodation coefficient on condensation sink is illustrated in Fig. 3b where the condensation sink as a function of size is displayed for growth-factors of 1 and 1.5. For a mass accommodation coefficient of 0.01, the total sink is significantly smaller than that using an accommodation coefficient of 1.0 (Fig. 3a). Not only is the magnitude of the condensation significantly altered by choice of accommodation coefficient, but the influence of super-micron particles contributes more significantly to the total removal of condensable vapours and a bimodal sink results.

4.3. Growth-rates and vapour concentrations

Using eqs. (3 and 4) we can estimate vapour concentrations and the source rate of condensable vapour for these case studies. However, calculation of these concentrations depends on assumptions of the properties of the condensable vapour such as molecular mass, diffusion coefficient and mass accommodation coefficient. As an example we have considered different growth-rates at different temperatures in order to able to estimate the effect of different parameters. The summary of the effect of parameter choice on the estimated concentration of the condensable vapour is given in Table 1 where it is seen that the choice of molecular mass and diffusion coefficient have only minor influence on the result. Also the effect of the temperature is negligible. The only parameter significantly affecting the calculated vapour concentration is the mass accommodation coefficient. Dividing the value by a factor of 100 ($\alpha = 0.01$) requires $100\times$ more vapour to reproduce the observed aerosol growth. However if the mass accommodation coefficient is 0.01, also the condensation sink is about 100 times smaller, therefore, the effect of mass accommodation coefficient on source rate (Q) is negligible.

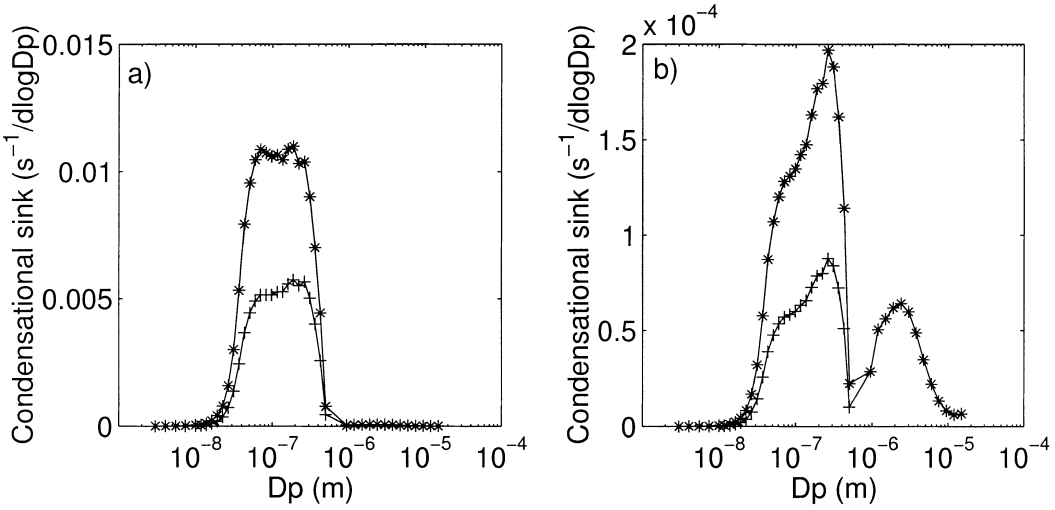

Fig. 3. Condensation sink as a function of size, Hyytiälä 14 April 1999. Sinks are calculated from DMPS and optical particle counter data. Two different hygroscopic growth factors (GF) are used for DMPS data evaluation: GF = 1.5 (+), GF = 1.0 (*). Mass accommodation coefficient 1.0 (a) and 0.01 (b).

Table 1. *The effect of molecular mass and mass accommodation coefficient of condensable vapour on vapour concentration as a function of growth rate and temperature*

dD/dt rate (nm/h)	M_v (amu)	α	T (K)	C (10^7 mol cm^{-3})
1	98	1	298.15	1.36
2	98	1	298.15	2.72
4	98	1	298.15	5.45
6	98	1	298.15	8.19
10	98	1	298.15	13.7
20	98	1	298.15	27.5
20	98	1	268.15	29.2
18	98	1	298.15	24.5
18	196	1	298.15	34.5
18	196	0.01	298.15	3420
18	98	0.01	298.15	2420
18	49	1	298.15	18.0

4.4. Case studies

From the BIOFOR campaigns, three events were selected from the April 1999 project since this corresponds to the period of peak frequency-of-occurrence. The analytical tools developed above are used to estimate the nucleation rates of new particles and the vapour source and concentration responsible for producing the observed growth in the three selected case studies.

First, we present the analysis made in Case I — 6 April 1999 (Julian Day 94) in detail. The growth-rate (diameter) was obtained from the DMPS data using the growth time from 3 nm to 10 nm (or sometimes 20 nm), and using eq. (4), the mean condensable vapour concentration can be obtained:

$$\frac{dD}{dt} = 2.2 \text{ nm/h} \rightarrow C \approx 3.0 \cdot 10^7 \text{ cm}^{-3}.$$

This value is good agreement with a recent, more detailed, model calculation of required vapour concentrations (Kulmala et al., 1998). Assuming pseudo steady-state, and using equation (1), with a calculated $CS = 2.5 \times 10^{-3}$ s^{-1}, the vapour source rate is approximately 7.5×10^4 cm^{-3} s^{-1}.

From the measured hygroscopic growth-factors, the soluble mass (or volume) fraction (X), assuming the soluble material to be ammonium sulphate, is determined. The soluble fraction associated with 10 nm, 15 nm and 20 nm size particles is presented in Fig. 4 for all three days. Solubilities are only presented for that period when the geometric mean diameter size in the growing mode corresponded to the 10, 15 and 20 nm solubility measurements. All cases show, that, as the new mode grows, the soluble fractions decreases significantly with a peak soluble fraction of 0.8 occurring for JD 104 at the start of the event, and minimum of

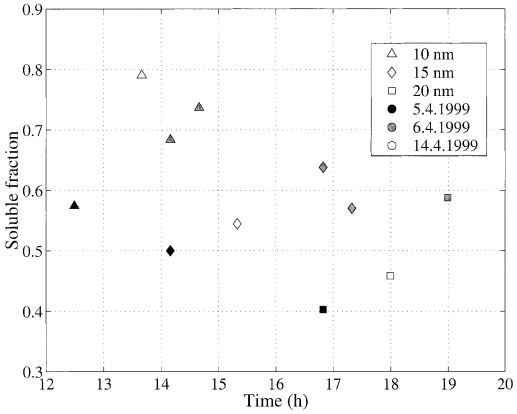

Fig. 4. Soluble fraction as function of time during three different days and for three different particles sizes. The data points corresponds to the times when growing nucleation mode peaks at the dry size selected. The error estimate for growth-factor is 0.05 and for the soluble fraction it is 0.1.

0.4 occurring for JD 95 in the latter stages of the event. For JD 94, when the peak in the growing mode passed through 10 nm, $X_{10\,\mathrm{nm}} = 0.69$, decreasing to $X_{20\,\mathrm{nm}} = 0.59$ as it passes through the 20 nm size.

Using the derived soluble mass fractions, the total mass of aerosol particles (M), and the soluble mass (M_2) and insoluble mass (M_1) the following expressions can be formulated (Kulmala et al., 1993). Subscripts 10 and 20 refer to particle diameter.

$$X = M_2/M, \qquad M = M_1 + M_2.$$

The mass of 10 nm and 20 nm particles is given, assuming similar composition, by M_{10} and M_{20}, respectively, where

$$M_{20} = 8M_{10}, \tag{19}$$

$$X_{20} = \frac{M_{2,10} + I_2 \cdot \Delta t}{M_{1,10} + M_{2,10} + (I_1 + I_2) \cdot \Delta t} = \frac{M_{2,20}}{M_{1,20} + M_{2,20}} = 0.6. \tag{20}$$

Here, I_i is the mass flux of condensable soluble ($i = 2$) or insoluble ($i = 1$) vapour. In practise, soluble vapour means sum of all soluble vapours and insoluble sum of all insoluble vapours.

$$X_{10} = \frac{M_{2,10}}{M_{1,10} + M_{2,10}} = 0.7. \tag{21}$$

After algebraic manipulation of (19–21), the soluble and non-soluble mass fluxes are related by the following relationship:

$$I_2 \approx 1.4 I_1.$$

Since I_2 = mass flux of soluble material, I_1 = mass flux of insoluble material, Δt = growth time (condensation growth), during the growth period, the soluble mass flux is somewhat higher than insoluble mass flux. Since the mass flux depends linearly on vapour concentration also the concentrations of condensable soluble and insoluble vapours are almost the same, the concentration of soluble material in gas phase being somewhat higher.

The coagulation sink for 3 nm particles was calculated to be $3 \times 10^{-4}\,\mathrm{s}^{-1}$, $N_3 = 2500\,\mathrm{cm}^{-3}$ and $\mathrm{d}N/\mathrm{d}t$ was $0.2\,\mathrm{cm}^{-3}\,\mathrm{s}^{-1}$. The formation rate of 3-nm particles from eq. (11) was calculated to be $0.95\,\mathrm{cm}^{-3}\,\mathrm{s}^{-1}$. The nucleation rate ($J_1$) from eq. (12) was 50–100 $\mathrm{cm}^{-3}\,\mathrm{s}^{-1}$. The concentration of N_1 was thus estimated (after some manipulation from eq. (9)) to be around 20,000–100,000 cm^{-3} .

Secondly we briefly describe the main results of other cases: Case Study II 14 April 1999 (Julian Day 104) and Case Study III 5 April 1999 (Julian Day 105). For the case study II, the growth-rate $\mathrm{d}D/\mathrm{d}t$ was 2.8–2.2 nm/h leading to a vapour concentration $C \approx (3.8\text{–}3.0) \cdot 10^7\,\mathrm{cm}^{-3}$. Since CS is $3 \times 10^{-3}\,\mathrm{s}^{-1}$, the source rate of the condensable vapour is approximately $11.4\text{–}9.0 \times 10^4\,\mathrm{cm}^{-3}\,\mathrm{s}^{-1}$. From the growth-factors, soluble fractions were calculated to be $X_{10\,\mathrm{nm}} = 0.78$ and $X_{20\,\mathrm{nm}} = 0.46$. For this case, the relative proportions of the soluble and non-soluble mass fluxes was estimated to be $I_2 \approx 0.71 I_1$.

The coagulation sink for 3-nm particles was $2.5 \times 10^{-4}\,\mathrm{s}^{-1}$, $N_3 = 3400\,\mathrm{cm}^{-3}$ and $\mathrm{d}N/\mathrm{d}t$ was $0.2\,\mathrm{cm}^{-3}\mathrm{s}^{-1}$. The formation rate of 3 nm particles from eq. (2) was calculated to be $1.1\,\mathrm{cm}^{-3}\,\mathrm{s}^{-1}$ and the nucleation rate (J_1) was 50–80 $\mathrm{cm}^{-3}\mathrm{s}^{-1}$, leading to an inferred concentration of N_1 in the region of 10,000–50,000 cm^{-3}. For the event on JD 105, the growth-rate, $\mathrm{d}D/\mathrm{d}t$, was 2.4–2.6 nm/h, leading to a condensable vapour concentration of $C \approx 3.4 \cdot 10^7\,\mathrm{cm}^{-3}$. Since CS was $3 \times 10^{-3}\,\mathrm{s}^{-1}$, the source rate of this vapour is approximately $10.2 \times 10^4\,\mathrm{cm}^{-3}\,\mathrm{s}^{-1}$. The soluble and insoluble fractions were calculated to be $X_{10\,\mathrm{nm}} = 0.59$ and $X_{20\,\mathrm{nm}} = 0.49$, resulting in the mass flux ratio $I_2 \approx 0.92 I_1$.

The coagulation sink for 3-nm particles was $2 \times 10^{-4}\,s^{-1}$, N_3 was $7000\,cm^{-3}$ and dN/dt was $0.2\,cm^{-3}s^{-1}$. The formation rate of 3 nm particles was, calculated from eq. (2), $1.6\,cm^{-3}s^{-1}$. The nucleation rate (J_1) was 10–100 $cm^{-3}\,s^{-1}$ leading to concentration of N_1 around 20,000–50,000 cm^{-3} .

4.5. *On the sensitivity of the results*

In order to be able to estimate the accuracy of this analysis, several sensitivity tests have been performed, e.g., in the previous section it has been illustrated that while source rate of the condensable vapour is, of course, independent of the mass accommodation coefficient, the vapour concentration depends strongly on mass accommodation coefficient and growth factor used.

The error estimates for observed growth-rate is 1–2 nm/h and for hygroscopic growth-factor 0.05. The condensation and coagulation sinks will vary by a factor of two during the event. Therefore our analysis gives typically order of magnitude estimation, e.g., for the ratio of soluble and insoluble mass fluxes the actual value of the ratio is not known. However, the ratio found to be around 1 is in the correct order of magnitude. The ratio is not likely to be more than 3 or less than 0.2.

Here we evaluate the sensitivity of derived nucleation rate, J_1, to different values of calculated coagulation sinks and estimated growth-rates. Fig. 5 illustrates the variation of J_1 as a function of growth-rate using different values for the coagulation sink. The effect of growth-rate is significant: varying the growth-rate from 2 nm/h to 6 nm/h reduces the formation rate by a factor of ten. Using the minimum coagulation sink, calculated from the data, instead of maximum, the nucleation rate decreases by a factor of 4.

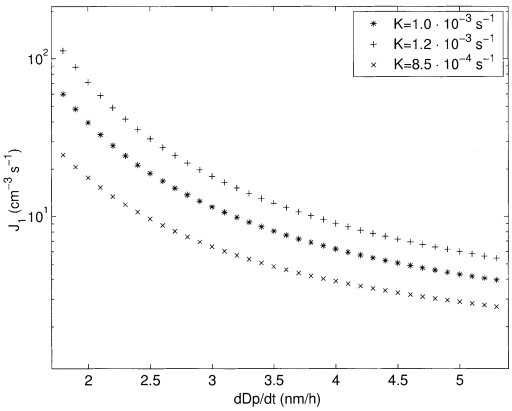

Fig. 5. Variation of particle formation rate (J_1) as a function of growth rate (nm/h). Three different values of coagulation sink (K) is used. Minimum $8.5 \times 10^{-4}\,s^{-1}$, average $1.0 \times 10^{-3}\,s^{-1}$, and maximum $1.2 \times 10^{-3}\,s^{-1}$, Hyytiälä 14 April, 1999.

5. Conclusion

In this study, the formation and growth of aerosol particles, and their soluble mass composition changes in the nucleation mode have been investigated using novel analytical tools. The analytical technique is applied to aerosol number size spectra only, resulting in estimates of nucleation rates and vapour source rates. From the size spectra diameter growth-rate, condensation and coagulation sinks can be calculated. Using growth-rates and condensation sinks, the concentration of condensable vapour and its source rate can be estimated. Using coagulation sinks together with measured number concentrations and apparent nucleation rates, the formation rates of 3 nm and 1 nm particles, as well as number concentration of 1 nm, particles can be estimated.

The method has been applied to three nucleation and growth event days during the 1999 spring-time BIOFOR campaign to elucidate particle formation rates and condensable vapour source strengths. The nucleation mode growth-rate is observed to be 2–3 nm/h, which corresponds to a condensable vapour concentration of $2.5–4 \cdot 10^7\,cm^{-3}$, and a vapour source rate of approximately $7.5–11 \times 10^4\,cm^{-3}\,s^{-1}$. Estimate of vapour source rate and concentrations using this technique agrees well with recent, more detailed, model studies by Kulmala et al. (1998) illustrating the usefulness of this approach to evaluate data giving reasonable results. The results here have been conducted for spring-time events, however, more recent analysis of summer-time data by Mäkelä et al. (2000) indicates that the growth-rate, at least in summer, can be almost 10 times higher that reported here, indicating the requirement for 10 times greater condensable vapour concentrations.

The formation rate of 3 nm particles is around

1 particles $cm^{-3}\,s^{-1}$ in all three days. The formation rate of 1 nm particles (actual nucleation rate) was estimated to be 10–100 particles $cm^{-3}\,s^{-1}$ and number concentration of 1 nm particles was shown to be around 10,000–100,000 particles cm^{-3}. These results are also in good agreement with the general results given by Kulmala et al. (2000).

Using the hygroscopic growth-factor data, the composition change of the growing new particle mode is analysed throughout the initial growth process. As a general result, the mass flux of insoluble vapours are of the same order of magnitude as the mass flux of soluble vapours, with a soluble to insoluble mass flux ratio varying from 0.7 to 1.4. Recent detailed aerosol and chemical evolution model studies (Pirjola and Kulmala, 2001) show that for these case studies, the sulphuric acid concentration produced through the oxidation of SO_2 is much less than that required to explain the observed growth and soluble fraction contribution. This indicates that a significant fraction of soluble mass is something other than sulphuric acid or ammonium sulphate, possibly a soluble organic acid.

6. Acknowledgements

The financial support from the European Commission, Program Environment and Climate under Contract ENV4-CT97-0405, and from the Academy of Finland is acknowledged. We are thankful to the reviewers for numerous useful comments.

REFERENCES

Allen, M. D. and Raabe, O. G. 1985. Slip correction measurments of spherical solid aerosol particles in an improved Millikan apparatus. *Aerosol Sci. Technol.* **4**, 269–286.

Aalto, P. Hämeri, K., Becker, E., Weber, R., Salm, J., Mäkelä, J. M., Hoell, C., O'Dowd, C. D., Karlsson, H., Hannsson, H.-C., Väkevä, M., Koponen, I., Buzorius, G. and Kulmala, M. 2001. Physical characterization of aerosol particles during nucleation events. *Tellus* **53B**, 344–358.

Birmili, W. and Wiedensohler A. 1998. The influence of meteorological parameters on ultrafine particle production at a continental site. *J. Aerosol Sci.* **29**, S1015–1016.

Charlson R. J., Lovelock, J. E., Andreae, M. O. and Warren, S. G. 1987. Oceanic phytoplankton, atmospheric sulphur, cloud albedo and climate. *Nature* **326**, 655–661.

Donaldson, K. XY Li and MacNee W. 1998. Ultra-fine (nanometer) particle-mediated lung injury. *J. Aerosol. Sci.* **29**, 553–560.

Fuchs, N. A. 1964. *The mechanics of aerosols*. Pergamon Press, London.

Fuchs, N. A. and Sutugin, A. G. 1971. Highly dispersed aerosol. In: Hidy, G. M. and Brock, J. R. (eds.), *Topics in current aerosol research*. Pergamon, New York.

Hämeri, K., Väkevä, M., Hansson, H.-C. and Laaksonen, A. 2000. Hygroscopic growth of ultrafine ammonium sulphate aerosol measured using a ultrafine tandem differential mobility analyser. *Journal of Geophysical Research* **105**, 22,231–22,242.

Hämeri, K., Väkevä, M., Aalto, P., Kulmala, M., Swietlicki, E., Seidl, W., Becker, E. and O'Dowd, C. D. 2001. Hygroscopic and CCN properties of aerosol particles in boreal forests. *Tellus* **53B**, 359–379.

Kavouras, I. G., Mihalopoulos, N. and Stephanou, E. G. 1998. Formation of atmospheric particles from organic acids produced by forests. *Nature* **395**, 683–686

Kulmala, M. 1988. *Nucleation as an aerosol physical problem*. PhD thesis. University of Helsinki, Department of Physics, Helsinki, Finland.

Kulmala, M., Vesala T. and Wagner P. E. 1993. An analytical expression for the rate of binary condensational growth. *Proc. Roy. Soc. Lond. A*. **441**, 589–605.

Kulmala, M., Toivonen, A., Mäkelä, J. M. and Laaksonen, A. 1998. Analysis of the growth of nucleation mode particles observed in Boreal forest. *Tellus* **50B**, 449–462.

Kulmala, M, Pirjola, L. and Mäkelä, J. M. 2000. Stable sulphate clusters as a source of new atmospheric particles. *Nature* **404**, 66–69.

Kulmala, M., Hämeri, K., Aalto, P. P., Mäkelä, J. M., Pirjola, L., Nilsson, E. D., Buzorius, G., Rannik, Ü, Dal Maso, M., Seidl, W., Hoffmann, T., Janson, R., Hansson, H.-C., Viisanen, Y., Laaksonen, A. and O'Dowd C. D. 2001. Overview of the international project on Biogenic aerosol formation in the boreal forest (BIOFOR). *Tellus* **53B**, 327–343.

Mäkelä, J. M., Aalto, P., Jokinen, V., Pohja, T., Nissinen, A., Palmroth, S., Markkanen, T., Seitsonen, K., Lihavainen, H. and Kulmala, M. 1997. Observations of ultrafine aerosol particle formation and growth in boreal forest. *Geophys. Res. Lett*. **24**, 1219–1222.

Mäkelä, J. M., Dal Maso, M., Pirjola, L., Keronen, P., Laakso, L., Kulmala, M. and Laaksonen, A. 2000. Characteristics of the aerosol particle formation events observed at a boreal forest site in southern Finland. *Boreal Environment Research* **5**, 299–313.

Nilsson, E. D. and Kulmala, M. 1998. The potential for

atmospheric mixing processes to enhance the binary nucleation rate. *J. Geophys. Res.* **103**, 1281–1389.

Nilsson, E. D., Rannik, Ü., Kulmala, M., Buzorius, G. and O'Dowd, C. D. 2001. Effects of the continental boundary layer evolution, convection, turbulence and entrainment on aerosol formation. *Tellus* **53B**, 441–461.

O'Dowd, C., McFiggins, G., Creasey, D. J., Pirjola, L., Hoell, C., Smith, M. H., Allan, B. J., Plane, J. M. C., Heard, D. E., Lee, J. D., Pilling, M. J. and Kulmala, M. 1999. On the photochemical production of new particles in the coastal boundary layer. *Geophys. Res. Letters* **26**, 1707–1710.

Pirjola, L., Kulmala, M., Wilck, M., Bischoff, A., Stratmann, F. and Otto, E. 1999. Effects of aerosol dynamics on the formation of sulphuric acid aerosols and cloud condensation nuclei. *J. Aerosol Sci.* **30**, 1079–1094.

Pirjola, L. and Kulmala, M. 2001. Development of particle size and composition distribution with aerosol dynamics model AEROFOR2. *Tellus* **53B**, 491–509.

Quant, F. R., Caldow, R., Sem, G. J. and Addison, T. J. 1992. Performance of condensation particle counters with three continous-flow designs. *J. Aerosol Sci.* **23**, S405-S408.

Seinfeld, J. H. and Pandis S. N. 1998. *Atmospheric chemistry and physics, from air pollution to climate change*. John Wiley & Sons, Inc. New York.

Stolzenburg, M. R. 1988. *An ultrafine aerosol size distribution measuring system.* PhD Thesis, University of Minnesota, Minneapolis MN, USA.

Stolzenburg M. R. and McMurry P. H. 1991. An ultrafine aerosol condensation nucleus counter. *Aerosol Sci. Technol.* **14**, 48–65.

Wiedensohler, A. 1988. An approximation of the bipolar charge distribution for particles in the submicron size range. *J. Aerosol Sci.* **19**, 387–389.

Winklmayr, W., Reischl, G. P., Lindner, A. O. and Berner, A. 1991. A new electromobility spectrometer for the measurement of aerosol size distributions in the size range from 1 to 1000 nm. *J. Aerosol Sci.* **22**, 289–296.

Väkevä, M., K. Hämeri, T. Puhakka, E. D. Nilsson, H. Hohti and Mäkelä, J. M. 2000. Effects of meteorological processes on aerosol particle size distribution in an urban background area. *J. Geophys. Res.* **105**, 9807–9821.

Weber, R. J., Marti, J. J., McMurry, P. H., Eisele, F. L., Tanner, D. J. and Jefferson A. 1996. Measured atmospheric new particle formation rates: Implications for nucleation mechanisms. *Chemical Engineering Communications* **151**, 53–64

Weber, R. J., Marti, J. J., McMurry, P. H., Eisele, F. L., Tanner, D. J. and Jefferson A. 1997. Measurements of new particle formation and ultrafine particle growth rates at a clean continental site. *J. Geophys. Res.* **102**, 4375–4385.